

Preparation and characterization of ketoprofen and pentoxifylline agents based layered double hydroxides-chitosan nanohybride and its releasing control

A. A. G. El-Shahawy^{a,*}, W. Kamal^a, O. M. Sayed^b, W. M. A. El Roubay^a,
H. Y. Zahran^{c,d}, I. S. Yahia^{c,d}, S. I. El-Dek^a, A. A. Farghali^a

^aMaterials Science and nanotechnology Dept., Faculty of Postgraduate Studies for Advanced Sciences (PSAS), Beni-Suef University, Beni-Suef, Egypt

^bDepartment of Pharmaceutics and Industrial Pharmacy, Faculty of Pharmacy, Beni-Suef University, Beni-Suef, Egypt

^cResearch Center for Advanced Materials Science (RCAMS), King Khalid University, Abha 61413, P.O. Box 9004, Saudi Arabia

^dMetallurgical Lab., Nanoscience Laboratory for Environmental and Bio-medical Applications (NLEBA), Semiconductor Lab., Physics Department, Faculty of Education, Ain Shams University, Roxy, 11757 Cairo, Egypt

The suggested research focused on the construction of a nanocomposite containing organic-inorganic materials as a pharmaceutical shipper to provide a regulated and preserved release of Ketoprofen and Pentoxifylline to reduce its hazards. The study examined the kinetics and the adsorption isotherms of these agents on layered double hydroxides, chitosan, and chitosan-layered double hydroxide nanocomposites that were prepared chemically and identified by high resolution transmission electron microscope, X-ray diffraction, and Fourier transformation Infra-red Spectroscopy. The results showed controlled and continued free through layer hydroxides, chitosan and chitosan-layered hydroxides. Langmuir was the best for illustrating and fitting the sorption equilibrium of Ketoprofen and Pentoxifylline onto the layered double hydroxides, counteracting Freundlich in Chitosan and Chitosan-layered double hydroxide adsorbents. Chitosan-layered double hydroxides, layered double hydroxides, and Chitosan achieved complete release of Pentoxifylline only. Furthermore, Ketoprofen release from chitosan particles was first order, whereas Pentoxifylline release from chitosan-layered double hydroxide complex was zero order. As a final point, the tested nanocarriers restricted the release of Ketoprofen and Pentoxifylline meticulously.

(Received December 6, 2019; Accepted April 20, 2022)

Keywords: Chitosan, Ketoprofen, Layered double hydroxides, Nanohybride, Pentoxifylline, Sustain release

1. Introduction

Ketoprofen (KTP) capsule formulations are the most commonly used nonsteroidal anti-inflammatory drugs (NSAIDs) for arthritis treatment [1]. However, using KTP for a long time with high doses increases the risk of a fatal heart attack and stroke, and can cause stomach or intestinal bleeding [2]. Although Pentoxifylline (PENT) is a xanthine derivative and it works by making red blood cells more flexible, which helps to improve blood flow with tolerance to mild side effects [3], PENT is a highly water-soluble and short-half-life drug [4], so, developing a carrier to ease such effects and sustain the release of KTP and PENT is desirable.

Recently, the use of inorganic nanoparticles in drug delivery systems has gotten a lot of attention because of their versatile properties such as wide availability; good biocompatibility, and rich surface functionality [5]. In addition, nanocarriers targeted and delivered drugs to the desired site of action, which is valuable in studies involving the delivery of chemotherapeutic agents in cancer therapy [6]. Moreover, nanoparticle-based drug delivery systems can quietly release the

* Corresponding author: samaa@psas.bsu.edu.eg
<https://doi.org/10.15251/DJNB.2022.172.527>

loaded drugs to maintain concentrations at the desired levels for an extended period [7]. To date, a multitude of inorganic nanoparticles have been extensively employed in drug delivery studies, including iron oxide [8, 9], silica [10], hydroxyapatite [11, 12], gold [13], carbon nanotubes [14], dendrimers [15], quantum dots [16, 17], and layered double hydroxides [18–19].

Layered double hydroxides (LDHs), or anionic clays, are a class of synthetic two-dimensional lamellar compounds with positive-charged layers and charge-balancing anions placed in the interlayer region [20]. LDHs have the general formula $[M_{1-x}^{2+}M_x^{3+}(\text{OH})_2]^{x+}(\text{A}_x/n^{n-})_m \cdot m\text{H}_2\text{O}$, where M^{2+} and M^{3+} are divalent and trivalent mineral ions, A_n and m are anion, and m is the amount of water in the inter-lamellar region [21]. Diclofenac was intercalated into Mg Al–Cl LDHs and Mg Al–CO₃ LDHs for oral drug delivery [23], and these nanocomposites demonstrated drug release control properties. Further, many successful intercalations have been presented with different therapeutic compounds, comprising conjugated linoleic acid [24], indole-3-acetic acid [25], gallic acid [26], ascorbic acid, retinoic acid, and α -tocopherol [27]. LDH nanomaterials show low cytotoxicity, excellent biocompatibility, and have several bio-applications [28].

Actually, chitosan is one of the most widely used cationic polysaccharides due to its nontoxicity, biocompatibility, and biodegradability with permeation enhancing properties [29]. Feng Cao et al. investigated Chitosan-glutathione-glycylsarcosine-LDH (CG-GS-KDH) active targeting intercalated nanocomposites as novel carriers for the treatment of mid-posterior diseases [30]. In addition, Pei-Ru et al. designed a study for photodynamic therapy (PDT) using chitosan coated Mg Al-LDH nanoparticles as the delivery system [31].

In the same sense, the present study concentrated on the preparation of a nanocomposite comprising organic compounds as a drug carrier to give controlled and sustained drug release of insoluble water (KTP) and highly water soluble (PENT). In extension, the research investigated the adsorption isotherms of these drugs on three adsorbent delivery systems: LDH, Chitosan, and Chitosan-LDH nanocomposites.

2. Materials and methods

2.1. Materials

Sodium hydroxide (NaOH), hydrochloric acid (HCl), acetone, aluminium nitrate (Al (NO₃)₂·9H₂O), zinc nitrate (Zn (NO₃)₂·6H₂O), methanol, acetic acid, 1-Propanol, β -alanine, mono-potassium phosphate (KH₂PO₄), and NaH₂PO₄·12H₂O were purchased and used as received without further purification. Peel shrimp were collected for use as a precursor for Chitosan.

2.2. Preparation of Chitosan

Chitosan was prepared by peeling shrimp following [32]. The purchased peeled shrimp were washed in warm water to eliminate impurities and dried for 24 hours. To reduce minerals and calcium carbonate, the cleaned shrimp peel was immersed in 1N (3–4%) HCl for 24 hours at room temperature, solid-solvent (1–15w/v), filtrated under a vacuum pump, washed several times, and dried. The dematerialized peel was interacted with 3.5% sodium hydroxide, Peel-sodium hydroxide (1-10 w/w) at 65 °C for 2 hours under mechanical shaking, filtered and washed for a half hour. For decolorization, the deproteinized peel was soaked in acetone for 2 hours at 50 °C under stirring for 2 hours, filtered under vacuum, and dried for 2 hours at 30 °C in an oven to give chitin. Deacetylation: the decolorized peel was washed and steeped in 50% of Sodium Hydroxide for 2 hours at 115 °C, solid-solvent (1-15). The deacetylated chitin was washed, filtered, and dried for 24 hours at 60 °C; the produced chitosan was studied by different methods.

2.3. Preparation of Al Zn LDH-Chitosan

A Zn-LDH-Chitosan composite was created by intercalating Chitosan into the Al Zn LDH using the co-precipitation method; a mixture of Al (NO₃)₃·9H₂O and Zn (NO₃)₂·6H₂O (Al/Zn=1/3 molar ratio) was dissolved in a solution of distilled water, 10 ml of 1-propanol, and 30 ml of Chitosan (0. The mixture was transferred into a Teflon-lined autoclave and heated at 120 °C

for 18 hours. The precipitate was filtered, washed numerous times to remove inorganic ions, and dried in a vacuum for 24 hours at 60°C.

2.4. Characterization of the prepared materials

Using Cu K radiation ($\lambda = 1.54$) in the 2-theta scan range of 5–80°, the X-ray diffraction (XRD) technique was used to characterize the crystallinity and phases of the materials. Fourier transformation infra-red (FTIR) spectra were recorded on the Bruker Vertex 70 FTIR spectrometer in the range from 400 to 4000 cm^{-1} . High-resolution transmission electron microscope (HRTEM) images were acquired using the JEM-2100 (JEOL, Japan) with an acceleration voltage of 200 kV. Also, field emission scanning electron microscope images (FESEM; JSM 6400 device, IEQL) were obtained.

2.5. Drugs loading and release

Sorption experiments were performed in 100 ml conical flasks containing 50 ml of various concentrations (2, 4, 6, 8, 10, 12, 20 mmolar) of (KTP) drug with molecular formula $\text{C}_{16}\text{H}_{14}\text{O}_3$ and a molecular weight of 254.285 g/mol; 10mg of LDH was added to these concentrations. Flasks were shaken at room temperature for 24 hours, and then the samples were centrifuged at 4000 rpm for 15 minutes. A: Standard calibration curves were developed for each concentration by measuring the absorbance of KTP solution at a specific wavelength using a UV spectrophotometer (Shimadzu 2600-UV). The absorbance of the KTP was measured at $\lambda = 254$ nm. The same procedures were repeated for Chitosan and LDH-Chitosan adsorbents. Similarly, the absorbance of (PENT) drug with a molecular weight of 278.312 g/mol and molecular formula $\text{C}_{13}\text{H}_{18}\text{N}_4\text{O}_3$ was tested at $\lambda = 274$ nm.

2.5.1. Adsorption studies

2.5.1.1. Calculations of the adsorption equilibrium capacity by static adsorption test:

A stock solution of KTP (100 mM) was prepared and further diluted as mentioned. The batch adsorption experiments were conducted by adding 5 mg of LDH into 10 mL of each diluted concentration, and then the solutions were shaken on a temperature-controlled water bath shaker (SHZ-82A). All experiments were performed at room temperature (288 K) and pH 7 for 48 hours. After adsorption equilibrium, the solutions were centrifuged at 10,000 rpm for 6 minutes, and the final drug concentrations of supernatants were determined by measuring the maximum absorbance of the samples at the specific wavelength (KTP). The adsorption equilibrium capacity, or the adsorbed amount, was calculated from mass balance according to the following equation [33]:

$$q_e = \frac{(C_0 - C_e)V}{m} \quad (1)$$

C_0 and C_e are the initial and equilibrium concentrations of drugs in solutions (mg/L), V is the volume of solution (L), m is the mass of the adsorbent (g), and the same procedures were repeated for Chitosan and LDH-Chitosan adsorbents, and the adsorption behaviour of KTP was studied by a linear adsorption isotherm model by Freundlich and Langmuir. In a like manner, the steps were repeated with the (PENT) drug.

2.5.2. Drug release

Carefully weighed samples of drug-loaded complexes (equivalent to 20 mg) were suspended in 0.1M HCl (500 ml) and stirred for 2 hours. After that, the pH was raised to 7.4 and the mixture was shaken for another 5 hours. Aliquots were taken at regular intervals were removed from the mixture at regular intervals and diluted to fixed volumes using a buffer solution at pH 7.8. The amount of liberated KTP and PENT was determined from its UV-absorption at 254 nm and 274 nm, respectively.

3. Results and discussion

3.1. Structural and functional characterization

The first aim of the current study was to prepare and characterize three delivery drug systems, aforementioned. Figure 1 shows the X-ray diffraction patterns of the prepared materials and the loaded drugs. The peak position (angle of diffraction) indicates the crystal structure, while the crest height is a measure of the crystallinity. The XRD spectrum of Al Zn LDH (Fig. 1a) matched with ICDD card no. (00-058-0178) and illustrated characteristic diffraction peaks at $2\text{-theta} = 9.90^\circ$ and 19.874° that corresponded to the diffraction planes (003) and (006); the (006) peak marked the hydroxalcalite-type and well-ordered crystalline materials, while the (003) peak indicated the basal of an interlayer anion in LDH materials [34]. The observed peaks of LDH were matched closely with those in the literature [35]. The XRD of Chitosan (Fig 1b) exhibited two distinct and broad peaks at $2\text{-theta}=10^\circ$ and 20° due to (020) and (110), respectively; this may be explained by the regularity in a polymer chain due to stable intermolecular hydrogen bonds formed between the hydroxyl and the presented amino groups in Chitosan. On the other hand, the crystallinity of Chitosan-LDH was somewhat distorted; the XRD of Chitosan-LDH (Fig 1c) showed diffraction peak shifting of (003) and (006), specifying the synergy between Chitosan and LDH. In addition, it displayed diffraction peaks at different angles corresponding to (012), (015), (018), (110), and (113). Further, the double characteristic LDH diffraction peaks were noted at 60.8° and 62.2° , indicating a common layered hexagonal structural pattern, which has created an opportunity to exchange anions between layers to adapt in the interlayer space [36].

The XRD spectrum of pure KTP (Fig 1d) revealed a series of distinctive and intense peaks which were indicative of KTP crystallinity. Similarly, (Fig 1e) reflects the XRD of PENT with clear peaks and coordinates with literature. However, in the XRD of LDH-KTP (Fig. 1f) and Chitosan-KTP (Fig. 1g) and Chitosan-LDH-KTP (Fig. 1h), the diffraction peaks that corresponded to the KTP drug were not detected. Likewise, the diffraction peaks of PENT vanished, as shown in LDH-PENT (Fig. 1i), Chitosan-PENT (Fig. 1j) and Chitosan-LDH-PENT (Fig. 1k). The absence of the diffraction peaks of the two drugs might be due to drug loading and interference with the adsorbent materials might disturb the arrangement of the drug plans.

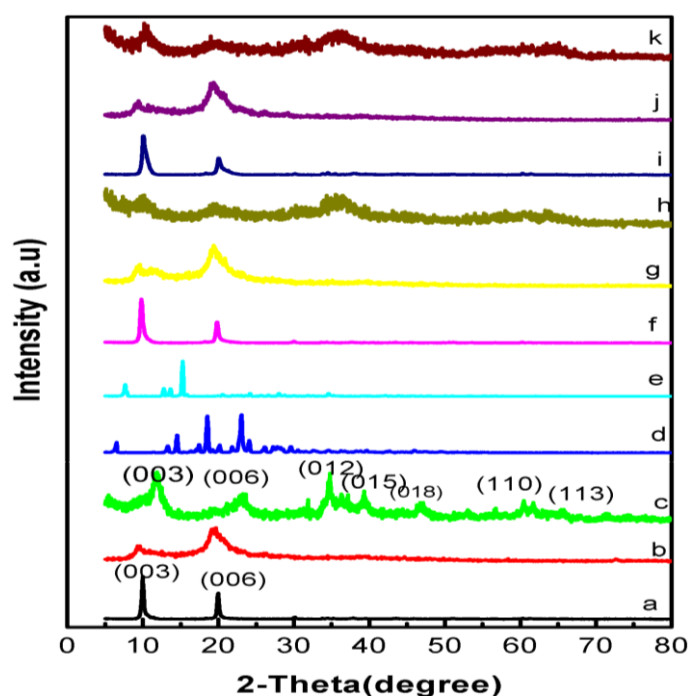


Fig. 1. XRD patterns of (a) LDH, (b) Chitosan, (c) Chitosan-LDH, (d) Ketoprofen, (e) PENT, (f) LDH-Ketoprofen, (g) Chitosan-Ketoprofen, (h) Chitosan-LDH-Ketoprofen, (i) LDH-PENT, (j) Chitosan-PENT and (k) Chitosan-LDH-PENT.

Fig. 2 shows the FTIR spectra of the formed materials and loaded drugs at different wave numbers. Zn-Al-NO₃ LDH displayed a wide band at 3444 cm⁻¹ that referred to ν (OH) group stretching vibration in the brucite-related sheets and the interlamellar water molecules [37]. The broadening of the band was attributed to the hydrogen bond formation. The band that appeared at 1380 cm⁻¹ was assigned to the ν_3 (antisymmetric) stretching vibration of the NO₃⁻ groups in the LDH interlayer [38]. The feeble band at 1634 cm⁻¹ could be assigned to the δ (H₂O) bending vibration of the interlayer water. The band approximately at 850 cm⁻¹ arose from O-M-O vibrations in the brucite-like layers (M=Al), whereas, the weak band at 650 cm⁻¹ was caused by the lattice vibration modes corresponding to the translation vibration of Zn-OH. The pure Chitosan spectrum showed basic characteristic peaks of Chitosan. The band at 3440 cm⁻¹ was related to NH stretching vibration, the peak at 1650 cm⁻¹ was assigned to CH₃ symmetrical in the amide group, a band at 1600 cm⁻¹ was attributed to the bending vibration of the N-H group, and the peak at 1629 cm⁻¹ was due to amide (I) [39]. The band at 2880 cm⁻¹ (C-H stretch), the weak band at 1654 cm⁻¹ (NH₂ deformation), and the band at 1153 cm⁻¹ were assigned to (bridge-O-stretch) [40]. The Chitosan-LDH spectrum illustrated peaks close to 3440 and 1382 cm⁻¹; almost as they appeared in the LDH spectrum; in addition, a peak shifting occurred at 1640 cm⁻¹. The FTIR spectrum of KTP reflected bands for C=O stretching vibration of acid, C=O stretching vibration of ketone, O-H band, and C=C stretching vibration of the aromatic ring appeared at 1698, 1372, 2981, and 3200 cm⁻¹, respectively [41]. The PENT spectrum exhibited characteristic bands at 2867, 1708, and 1658 cm⁻¹ for -CH₂-, -CO-, and amide-CO stretching mode [42]. Bands were also presented at 1359 cm⁻¹ for CH₃ deformation and 750 cm⁻¹ for (CH₂)_n-skeletal vibration. Some tenuous changes in the FTIR spectrum for PENT and KTP, indicating no chemical interaction between the drugs and the LDH, Chitosan, and LDH-Chitosan after loading.

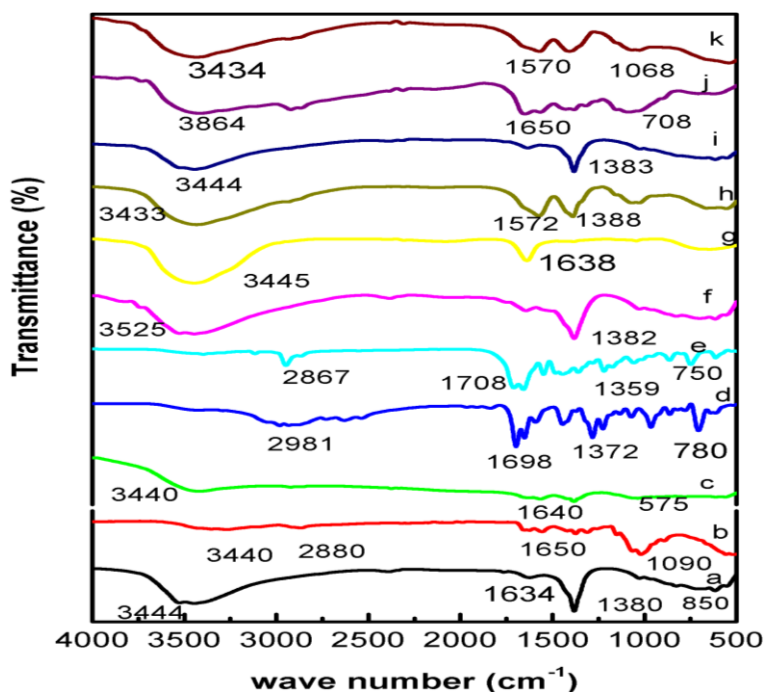


Fig. 2. FTIR spectra of (a) LDH, (b) Chitosan, (c) Chitosan-LDH, (d) Ketoprofen, (e) PENT, (f) LDH-Ketoprofen, (g) Chitosan-Ketoprofen, (h) Chitosan-LDH-Ketoprofen, (i) LDH-PENT, (j) Chitosan-PENT and (k) Chitosan-LDH-PENT.

The surface morphology of LDH (Fig. 3a) was examined using field emission scanning electron microscopy. LDH material existed in various sizes and appeared as a non-uniform sheet structure with different thicknesses and without any specific shape. It is possible to observe lamellar crystal formation with superposition of the layers, which disappeared in Chitosan-LDH Fig. (3b). After combination with Chitosan, this structure was transformed into agglomerate consisting of curled-up sheet like structures. The LDH particle size was markedly reduced in comparison with the starting material. In addition, the combination resulted in a change in the surface morphology of LDH with an irregular granular structure. High-resolution micrographs of the internal structure of LDH (Fig. 4a) and Chitosan-LDH (Fig. 4b) were obtained using TEM.

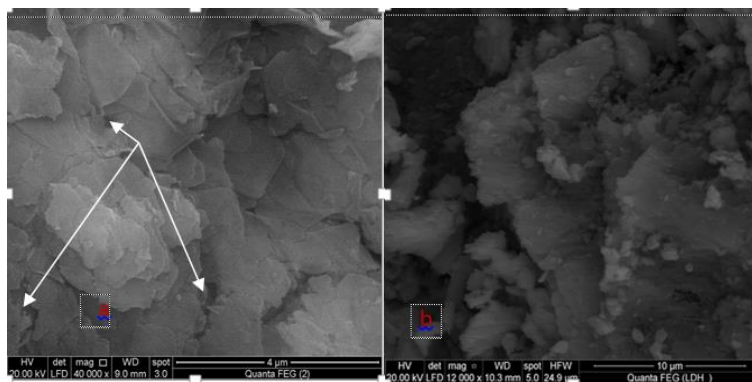


Fig. 3. FESEM (a) LDH and (b) Chitosan-LDH.

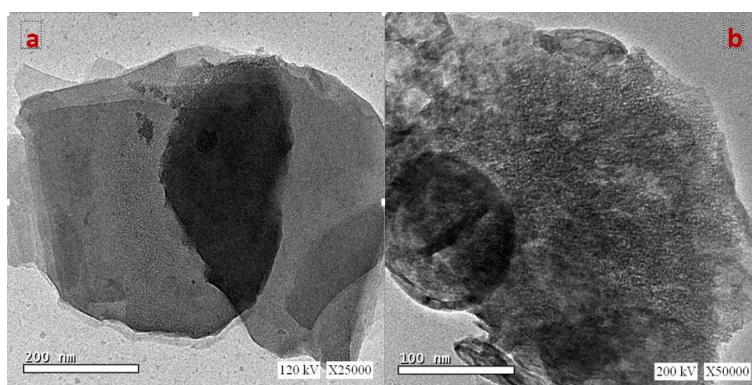


Fig. 4. HRTEM (a) LDH and (b) Chitosan-LDH.

3.2. Adsorption isotherm study

The second objective of this research was to investigate the adsorption isotherms of insoluble water KTP and highly water-soluble PENT on the three aforementioned adsorbents. In addition, to assess the potential use of these adsorbents as carriers to provide controlled and possibly sustained drug release.

Indeed, the most convenient method for describing the adsorption systems and assessing their behaviour is to have an idea of adsorption isotherms, where it is possible to express the results of experimental sorption measurements in the form of equilibrium sorption isotherms [43]. Equilibrium sorption isotherm studies are important in the design of sorption systems because they provide useful information about the interactions between the adsorbate and the adsorbent and determine the thermodynamic parameters and the maximum adsorption capacity, which is the ratio between the quantity sorbed and that remaining in the solution at a fixed temperature at

equilibrium. The equilibrium sorption isotherms are characterized by certain constants whose values express the surface properties and affinity of the sorbent [44].

In the current study, controlling the release of KTP and PENT from the prepared materials was investigated by an adsorption isotherm, and as such, Freundlich and Langmuir isotherm models were adopted to describe the experimental equilibrium adsorption data. The Freundlich isotherm model is the earliest known relationship describing non-ideal and reversible adsorption, which can be applied to multilayer adsorption with an interaction between the adsorbed molecules. The model revolves around an assumption concerning the adsorption onto heterogeneous surfaces by a uniform energy distribution and reversible adsorption, and assumes that the adsorption energy exponentially drops at the finishing point of the adsorption centres of an adsorbent. The linear expression of the Freundlich isotherm model can be illustrated as Equation (2) [45]:

$$\ln q_e = \ln K_F + \frac{1}{n} \ln C_e \quad (2)$$

C_e is the equilibrium concentration of drug in solution; K_F is a Freundlich constant related to adsorption capacity (L/g); in other words, the ability of the adsorbent to adsorb, while (n) is a constant concerned with the tendency of the adsorbate to be adsorbed, or it is the surface heterogeneity factor (g/L). The Freundlich constants are empirical constants that depend on many environmental factors; the value of $1/n$ indicates the intensity of adsorption or surface heterogeneity, revealing higher heterogeneity as it gets closer to zero. If $1/n < 1$, it indicates favourable adsorption. The Freundlich constants can be calculated from the plots of $\ln q_e$ vs. $\ln C_e$. The intercept and slope of the Freundlich adsorption isotherm were determined from the intercept and slope of the Freundlich adsorption isotherm.

On the other hand, the Langmuir model quantitatively describes the formation of a monolayer adsorbate on the outer surface of the adsorbent, after which no further adsorption occurs. The model represents the equilibrium distribution of the adsorbate between the solid and liquid phases [46]. The Langmuir adsorption isotherm, the most widely used isotherm for the adsorption of pollutants from a liquid solution, is based on the following hypotheses: (1) monolayer adsorption; (2) adsorption takes place at specific homogeneous sites on the adsorbent; (3) no further adsorption can occur at that site; (4) the adsorption energy is constant and does not depend on the degree of occupation of an adsorbent's active centers; (5) the strength of the intermolecular attractive forces is believed to decrease rapidly with distance; (6) the adsorbent has a finite capacity for the adsorbent; (7) all sites are identical and energetically equivalent; (8) the adsorbent is structurally homogeneous; and (9) there is no interaction between the molecules adsorbed onto the neighbouring sites [47]. The linear expression of the Langmuir isotherm model can be illustrated as Equation (3) [48].

$$\frac{C_e}{q_e} = \frac{C_e}{q_{max}} + \frac{1}{q_{max}K_L} \quad (3)$$

C_e is the solution's equilibrium concentration (mg/L), q_{max} is the maximum adsorption capacity (mg/g), and k_L is a Langmuir constant related to binding site affinity and adsorption energy (L/g). The Langmuir constants could be obtained from the plot of C_e/q_e vs. C_e .

The presented study reported the experimental results for the adsorption isotherms and the equilibrium absorbency values, which were gathered at different initial concentrations. Figs. (5 & 6) display Langmuir adsorption isotherms for KTP and PENT on the three adsorbents LDH, Chitosan, and LDH-Chitosan, while Figs. (7 & 8) exhibit Freundlich adsorption isotherms. In the Langmuir isotherm, the linear fit of the equilibrium amount of drug adsorbed onto the adsorbent nanoparticles (C_e/q_e , mg/g) was plotted as a function of the equilibrium drug concentration in the solution (C_e , mg/L), whereas in the Freundlich isotherm, a linear fit of the equilibrium amount of drug adsorbed onto the adsorbent nanoparticles ($\ln q_e$, mg/g) was plotted as a function of the equilibrium drug concentration in the solution ($\ln C_e$, mg/L). Additionally, the linear regression method using Origin 8.0 software was used for fitting the experimental data and direct determination of the isotherm model parameters, with the quality of fit assessed using the correlation coefficient (R^2), illustrated as Equation (4).

$$R^2 = \frac{\sum(q_m - \bar{q}_e)^2}{\sum(q_m - \bar{q}_e)^2 + \sum(q_m - q_e)^2} \quad (4)$$

q_m is the constant obtained from the isotherm model, q_e is the equilibrium capacity obtained from experimental data, and is the average of q_e or model equilibrium capacity data. If the data from the model is similar to the experimental data, the value of R^2 will be large; otherwise, the value of R^2 will be small.

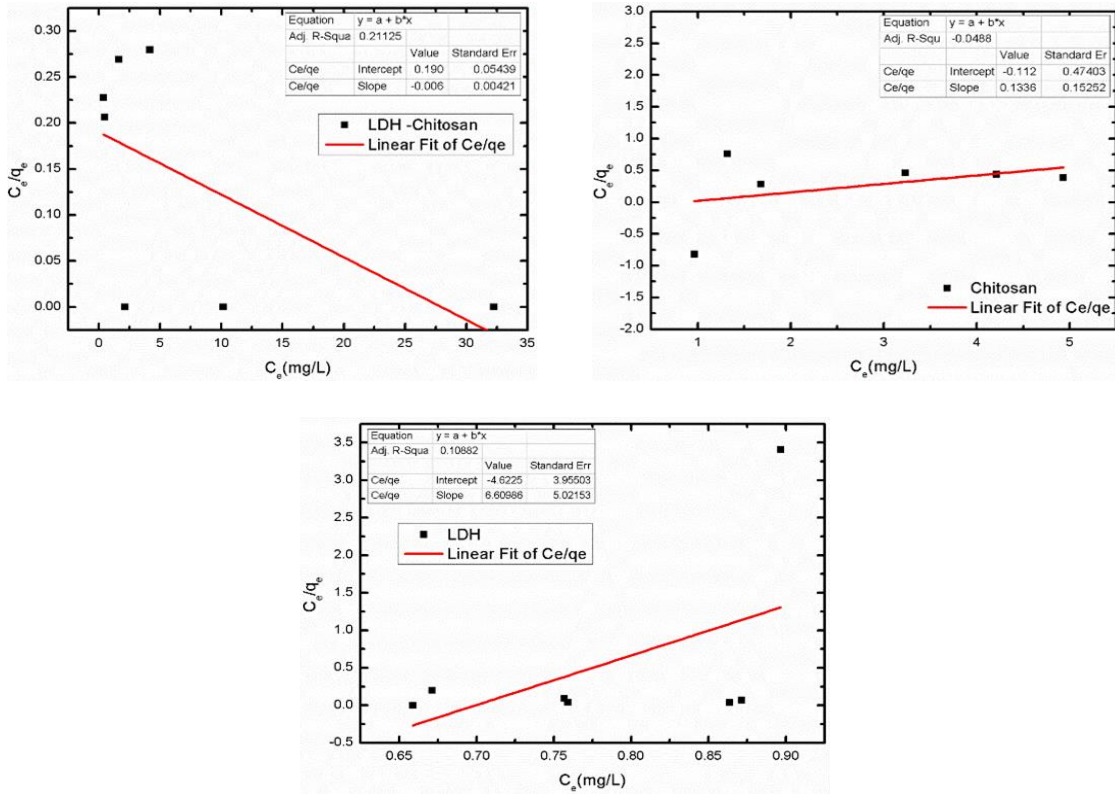


Fig. 5. Langmuir adsorption isotherm for KTP on LDH, Chitosan, LDH-Chitosan

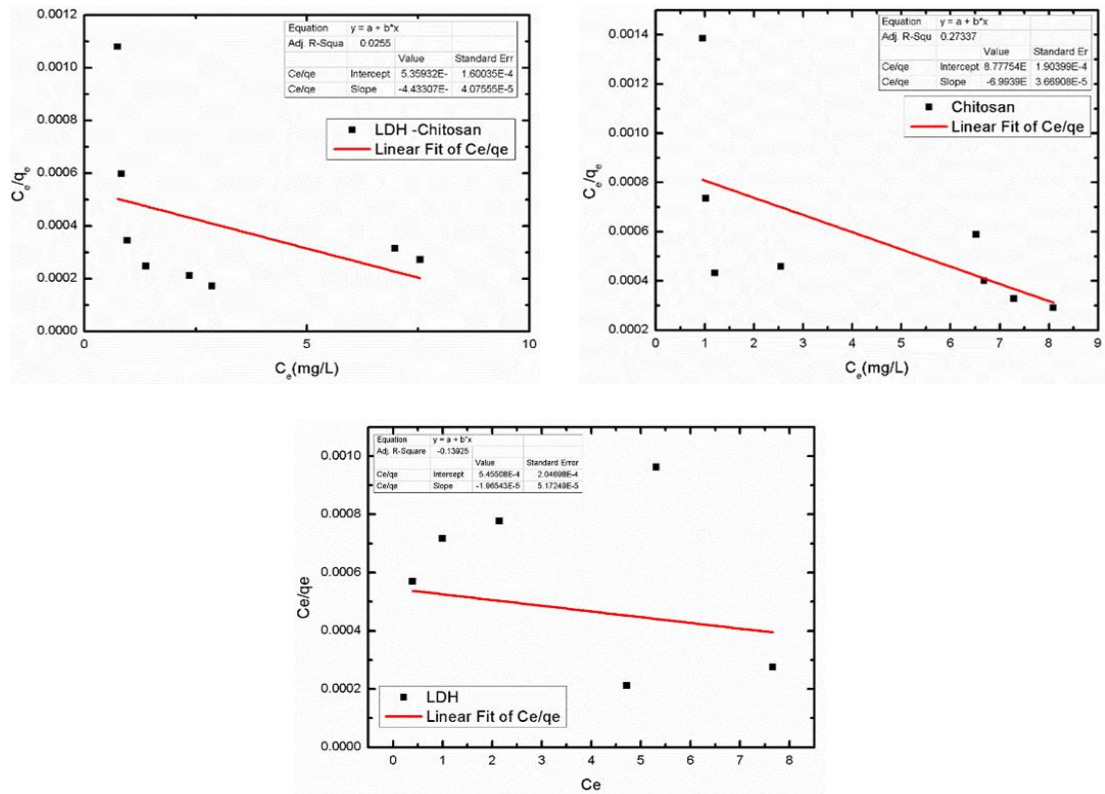


Fig. 6. Langmuir adsorption isotherm for PENT on LDH, Chitosan, LDH-Chitosan

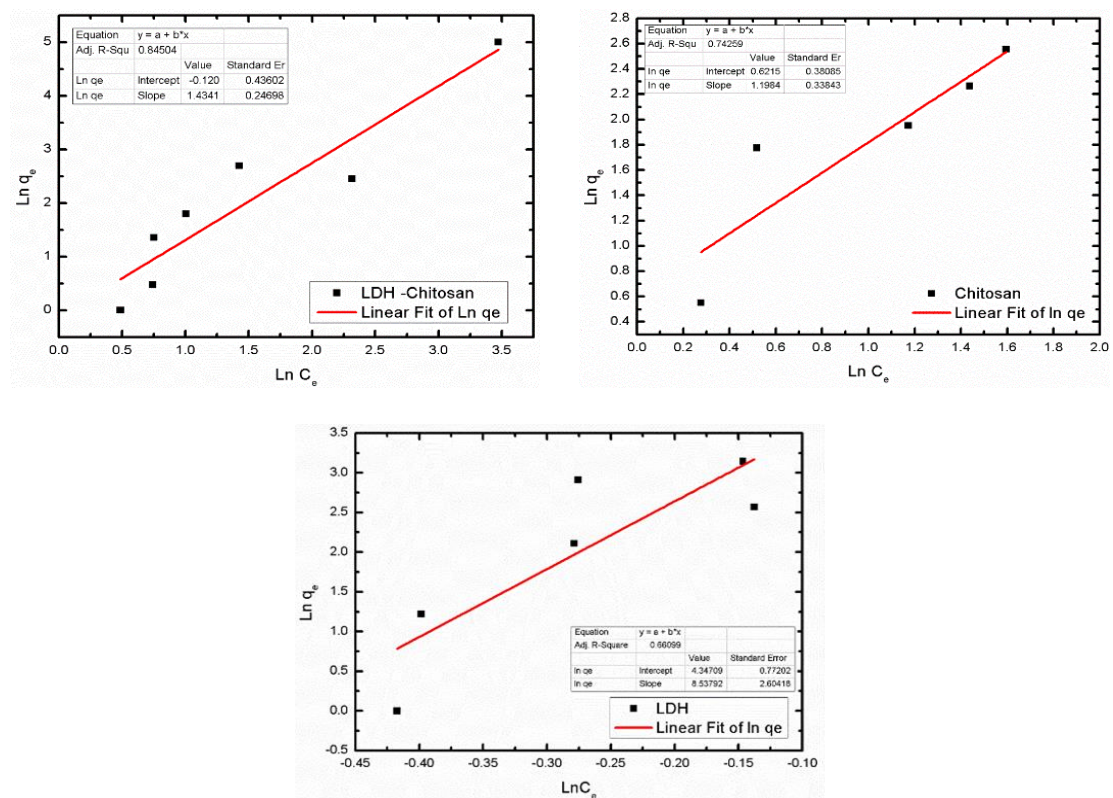


Fig. 7. Freundlich adsorption isotherm for KTP on LDH, Chitosan, LDH-Chitosan

Table 1 displays the reported correlation coefficients (R^2) values (goodness of fit), which were computed by linear regression of the Langmuir and Freundlich equations. The results disclosed that the R^2 values were in the following order: Langmuir > Freundlich in the case of LDH; the high value of R^2 suggested that the Langmuir model was better than Freundlich for describing and fitting the sorption equilibrium of KTP and PENT onto the LDH adsorbent and predicted monolayer sorption behavior; these results were boosted by studying the surface morphology where the observed LDH particles under SEM displayed shaped sheets as shown in Fig. (3a). In addition, several heterogeneous microscopic pores (dark parts, referred to by arrows) could be seen, which are identified to produce a wider surface area for adsorption, making the LDH nanoparticles a well-supported material. In contrast, the Freundlich model presented a higher R^2 than Langmuir in the case of chitosan and chitosan-LDH adsorbents, i.e., the Freundlich design fitted the experimental data well and predicted heterogeneous adsorption of adsorbents. Furthermore, the heterogeneous surface of the Chitosan-LDH nanoparticles is obvious from Fig. (3b) coordinates well with the Freundlich isotherm model.

Table (1): Correlation Coefficients of fitted line from different adsorption isotherms

Drug	Platform	R^2 of isotherm	
		Langmuir	Freundlich
Ketoprofen	LDH	0.32182	-0.21208
	Chitosan	0.1213	0.74259
	Chitosan - LDH	-0.17857	-0.65348
Pentoxifylline	LDH	0.93261	0.68359
	Chitosan	0.71031	0.92321
	Chitosan - LDH	0.99999	1

3.3. Release studies

Generally, drug release refers to the process in which drug solutes migrate from the initial position in the polymeric system to the polymer's outer surface and then to the release medium. This seemingly simple process is affected by multiple complex factors such as the physicochemical properties of the solutes (solubility, stability, charges, interaction with matrix), the structural characteristics of the material system (composition, structure, swelling, degradation), the release environment (pH, temperature, ionic strength, enzymes), and the possible interactions between these factors [48].

The current study utilized biodegradable materials such as LDH, chitosan, and Chitosan-LDH nanocomposites for sustaining release. Fig. 8 displays the release profile of KTP and PENT from different platforms at a constant temperature of 37 ± 0.5 °C. It is worth mentioning that the pH was adjusted from acidic (pH 1.2) for 2 hours to alkaline (pH 7.4) for 5 hours to simulate passage through the stomach and intestine conditions, i. e., gastrointestinal tract (GIT). It is noted that the release percent of the tested drug increased as the shaking time and concentration increased. In addition, the rate curves showed a controlled release pattern and exhibited variations in the initial releasing rates within the first 50 minutes of shaking time, followed by a relatively slow phase that appeared after 100 minutes, and finally attaining equilibrium. Furthermore, it was observed that the equilibrium time was up to 120 minutes, and an increase in the shaking time to more than 150 minutes did not change the release rates.

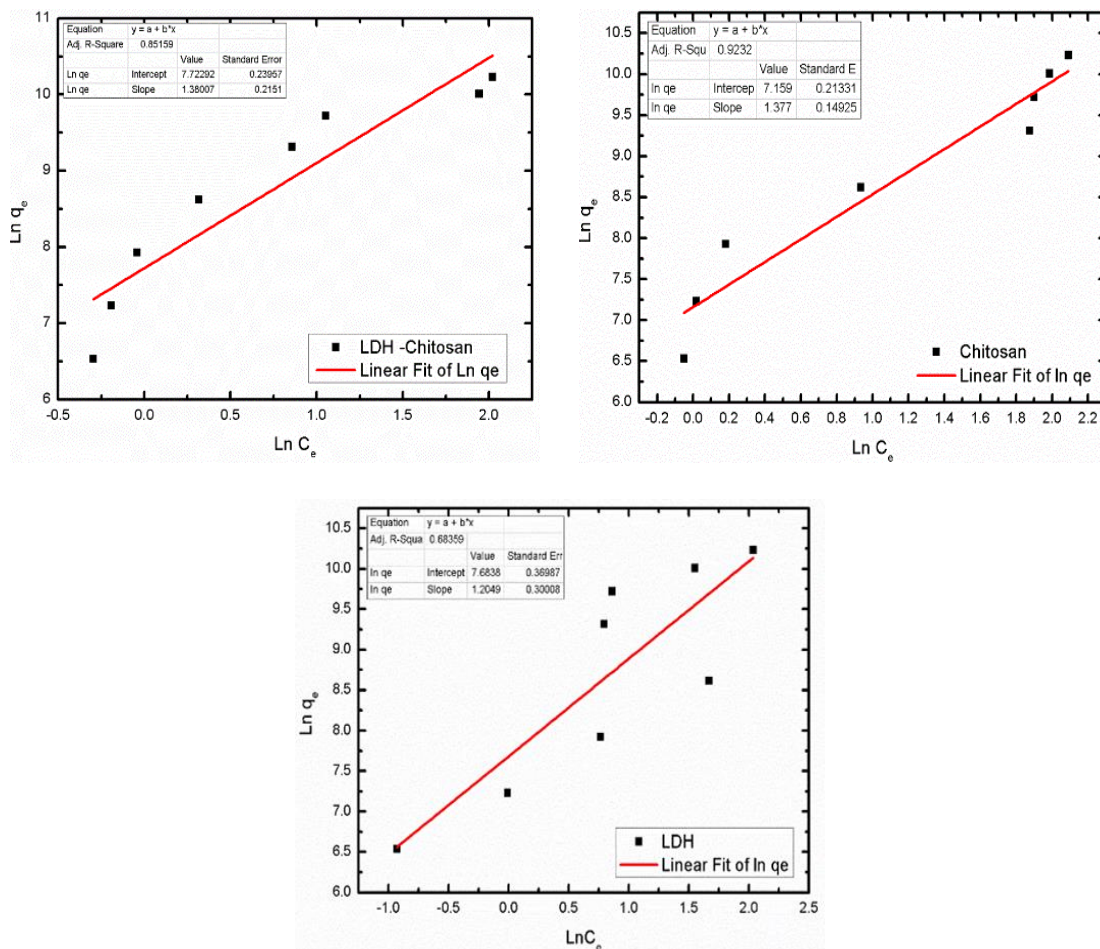


Fig. 8. Freundlich adsorption isotherm for PENT on LDH, Chitosan, LDH-Chitosan

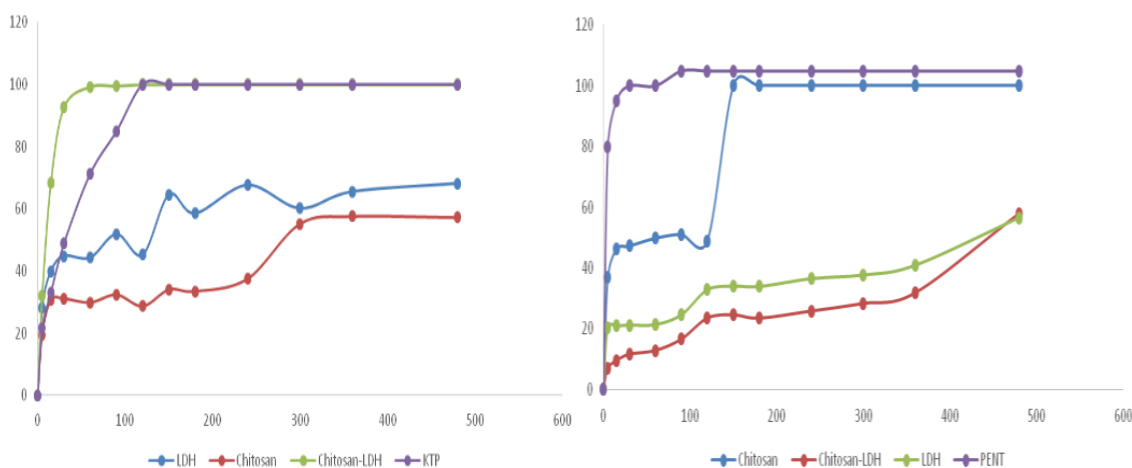


Fig. 9. Release profiles of KTP and PENT its adsorption complexes.

In agreement with [49], the results revealed that the release percent of KTP was in the following order: Chitosan-LDH complex > LDH > Chitosan. The chitosan-LDH composite achieved complete drug release faster than free KTP drug powder; this could be attributed to the disorder of the loaded drug plans, which was confirmed by the absence of KTP diffraction patterns within the adsorbent materials, as shown in Fig. 1. As a result, the dissolution and release rate

increased. On the other hand, LDH achieved a KTP release rate of less than 60%, which could be attributed to the slow ion exchange process and the rigidity of the layers of the LDH during drug diffusion path [50]. Generally, solute diffusion, polymeric matrix swelling, and material degradation are the major driving forces for solute transport from drug-containing polymeric matrices. The steady and gradual release of KTP from Chitosan might be attributed to the release mechanism either by drug molecule diffusion or by polymer matrix degradation. Further, from Fig. (8), one can observe the initial burst release of KTP; this was owing to the drug molecules dispersing close to the nanoparticle surface. In addition, the molecules of the drug would diffuse easily through the surface or pores of nanoparticles. The surface area, the porosity, and the volume measurements of the three adsorbents should be obtained in this research. In contrast, in the case of PENT, only Chitosan particles achieved complete release of PENT after a slow release period in the acidic medium. This could be attributed to the swelling of Chitosan to form a network that hindered the release in the acidic medium and collapsed in the alkaline medium afterward, leading to the fast and complete release of PENT. Meanwhile, both LDH and Chitosan-LDH complexes showed an incomplete release of PENT; this was probably due to the characteristics of the ion-exchange reaction in both acidic and basic conditions, i.e., the equilibrium process and the interlayer anions could not be exchanged completely [51].

Table (2): Release kinetics of KTP and PENT

Drug	Platform	R ² of fitted curve		
		Zero order	First Order	Diffusion
Ketoprofen	LDH	0.555234	0.67443	0.771346
	Chitosan	0.748224	0.816538	0.81577
	Chitosan - LDH	0.652186	0.661107	0.799859
Pentoxifylline	LDH	0.812743	0.869027	0.885967
	Chitosan	0.652186	0.682811	0.799859
	Chitosan - LDH	0.89555	0.854443	0.866263

Finally, the presented study investigated the correlation coefficient of different release kinetics of KTP and PENT as recorded in Table 2. All complexes showed a drug release fitting the Kros-Peppas model of release, which is used to analyse the release of pharmaceutical polymeric dosage forms when the release mechanism is not well known or when more than one type of release phenomenon could be involved [52]. Only PENT release from Chitosan-LDH showed a good fit with Higuchi diffusion, which usually deals with water soluble drug dissolution and diffusion from matrices [53]. Further, KTP release from Chitosan particles exhibited a first order while PENT from the Chitosan-LDH complex achieved a zero order release.

4. Conclusion

In short, to limit the side effects of the KTP PENT drug, the current study provides controlled and continued free through LDH, Chitosan, and Chitosan-LDH. Langmuir was the best for describing and fitting the sorption equilibrium of KTP and PENT onto the LDH, in contrast to Freundlich in Chitosan and Chitosan-LDH adsorbents. Chitosan-LDH, LDH, and Chitosan had the highest percentage of KTP released, while Chitosan particles had the lowest percentage of PENT released. In addition, KTP release from chitosan particles exhibited a first order, whereas PENT from the Chitosan-LDH complex achieved a zero order release.

Acknowledgements

The authors are thankful to all members of the Materials Science and Nanotechnology Dept., Faculty of Postgraduate Studies for Advanced Sciences (PSAS) and Beni-Suef University Egypt for supporting the preparation of the nanomaterials. Furthermore, all members of the Central Lab for Characterization and the Department of Pharmaceutics and Industrial Pharmacy, Faculty of Pharmacy, Beni-Suef University for drug release research.

References

- [1] D. Nagi Reddy et al., *AAPS Pharm. Sci. Tech.*, 1 (2018).
- [2] P. A Gum et al., *Journal of the American College of Cardiology* 41(6), 961 (2003); [https://doi.org/10.1016/S0735-1097\(02\)03014-0](https://doi.org/10.1016/S0735-1097(02)03014-0)
- [3] A. Bacher et al., *Acta anaesthesiologica scandinavica* 49(1), 41 (2005); <https://doi.org/10.1111/j.1399-6576.2004.00547.x>
- [4] A. Rahim Safwan et al., *Drug design, development and therapy* 9, 1843 (2015).
- [5] Z. Al Othman et al., *Trans. Tech. Publications*, 21 (2013).
- [6] F. Uddin et al., *International journal of nanomedicine* 12, 7291 (2017).
- [7] F. Benyettou et al., *ACS applied materials & interfaces* 460, 40006 (2017); <https://doi.org/10.1021/acsami.7b11423>
- [8] I. Khan et al., *Arabian Journal of Chemistry*, (2017).
- [9] J. Estelrich et al., *International journal of molecular sciences* 16(4), 8070 (2015); <https://doi.org/10.3390/ijms16048070>
- [10] M. Vallet-Regí et al., *Molecules* 23(1), 47 (2017); <https://doi.org/10.3390/molecules23010047>
- [11] M. Ramli et al., *International journal of nanomedicine* 8, 297 (2013); <https://doi.org/10.2147/IJN.S38858>
- [12] N. Kottegoda et al., *ACS nano* 11(2), 1214 (2017); <https://doi.org/10.1021/acsnano.6b07781>
- [13] E.C Dreaden et al., *Therapeutic delivery* 3(4), 457 (2012); <https://doi.org/10.4155/tde.12.21>
- [14] A. Bianco et al., *Current opinion in chemical biology* 9(6), 674 (2005); <https://doi.org/10.1016/j.cbpa.2005.10.005>
- [15] L. E. Euliss et al., *Chemical Society Reviews* 35(11), 1095 (2006); <https://doi.org/10.1039/b600913c>
- [16] C. E. Probst et al., *Advanced drug delivery reviews* 65(5), 703 (2013); <https://doi.org/10.1016/j.addr.2012.09.036>
- [17] E. C. Cho et al., *Trends in molecular medicine* 16(12), 561 (2010); <https://doi.org/10.1016/j.molmed.2010.09.004>
- [18] X. Bi et al., *Pharmaceutics* 6(2), 298 (2014); <https://doi.org/10.3390/pharmaceutics6020298>
- [19] Y. Kuthati et al., *Applied Clay Science* 112, 100 (2015); <https://doi.org/10.1016/j.clay.2015.04.018>
- [20] J. I. Velasco et al., *Advances in Polymer Nanocomposites*, 91 (2012); <https://doi.org/10.1533/9780857096241.1.91>
- [21] J. J. Bravo-Suárez et al., *Chemistry of materials* 16(7), 1214 (2004); <https://doi.org/10.1021/cm034853c>
- [22] J. Chakraborty et al, *Trans. Tech. Publications*, 133 (2013).
- [23] E. Heraldy et al, *IOP Conference Series: Materials Science and Engineering*, 12026 (2016).
- [24] D. Paul et al., *Colloids and Surfaces B: Biointerfaces* 126, 426 (2015); <https://doi.org/10.1016/j.colsurfb.2014.12.046>
- [25] S-Feng Fu et al., *Plant signaling & behavior* 10(8), 1048052 (2015); <https://doi.org/10.1080/15592324.2015.1048052>

- [26] D. Dorniani et al., *International journal of nanomedicine* 7, 5745 (2012); <https://doi.org/10.2147/IJN.S35746>
- [27] S. Senapati et al., *Signal transduction and targeted therapy* 3(1), 7 (2018); <https://doi.org/10.1038/s41392-017-0004-3>
- [28] H. Zuo et al., *Modifying layered double hydroxide nanoparticles with peptide to penetrate blood brain barrier for gene delivery*, (2017).
- [29] R. C. F. Cheung et al., *Marine drugs* 13(8), 5156 (2015); <https://doi.org/10.3390/md13085156>
- [30] T. Xu et al., *International journal of nanomedicine* 13, 917 (2018); <https://doi.org/10.2147/IJN.S148104>
- [31] P.-R. Wei et al., *International journal of molecular sciences* 16(9), 20943 (2015); <https://doi.org/10.3390/ijms160920943>
- [32] R. Santa Cruz Martins de Queiroz Antonino et al., *Marine drugs* 15(5), 141 (2017); <https://doi.org/10.3390/md15050141>
- [33] Y. S. Ho et al., *Water, air, and soil pollution* 124(1-2), 141 (2000); <https://doi.org/10.1023/A:1005218411809>
- [34] J. H. Choy et al., *Angewandte Chemie International Edition* 39(22), 4041 (2000); [https://doi.org/10.1002/1521-3773\(20001117\)39:22<4041::AID-ANIE4041>3.0.CO;2-C](https://doi.org/10.1002/1521-3773(20001117)39:22<4041::AID-ANIE4041>3.0.CO;2-C)
- [35] B. Balcomb et al., *Chemistry Open* 4(2), 137 (2015); <https://doi.org/10.1002/open.201402074>
- [36] S. J. Mills et al., *Mineralogical Magazine* 76(5), 1289 (2012); <https://doi.org/10.1180/minmag.2012.076.5.10>
- [37] F. Cao et al., *International journal of pharmaceutics* 404(1-2), 250 (2011); <https://doi.org/10.1016/j.ijpharm.2010.11.013>
- [38] S. Babakhani et al., *Advanced Materials Research*, 1024 (2014); <https://doi.org/10.4028/www.scientific.net/AMR.1024.52>
- [39] N. Ahmed Mohamed et al., *International journal of molecular sciences* 13(9), 11194 (2012); <https://doi.org/10.3390/ijms130911194>
- [40] J. Sun et al., *Green Chemistry* 14(3), 654 (2012); <https://doi.org/10.1039/c2gc16335g>
- [41] M. L. Vueba et al., *International journal of pharmaceutics* 307(1), 56 (2006); <https://doi.org/10.1016/j.ijpharm.2005.09.019>
- [42] Z. Omid, *Dermatology online journal* 14(11), (2008).
- [43] X. Chen, *Information* 6(1), 14 (2015); <https://doi.org/10.3390/info6010014>
- [44] Y. S. Ho et al., *Process Biochemistry* 37(12), 1421 (2002); [https://doi.org/10.1016/S0032-9592\(02\)00036-5](https://doi.org/10.1016/S0032-9592(02)00036-5)
- [45] K. Y. Foo et al., *Chemical engineering journal* 156(1), 2 (2010); <https://doi.org/10.1016/j.ces.2009.09.013>
- [46] M. Noori Sepehr et al., *Arabian Journal of Chemistry* 10(5), 611 (2017); <https://doi.org/10.1016/j.arabjc.2016.07.003>
- [47] B. Meroufel et al., *J. Mater. Environ. Sci.* 4(3), 482 (2013).
- [48] *International Journal of Scientific and Research Publications* 6(4), 549 (2016).
- [49] M. Arshadi et al., *Water Resources and Industry* 6, 1 (2014); <https://doi.org/10.1016/j.wri.2014.06.001>
- [50] M. Sillion et al., *J. Optoelectron. Adv. M.* 12(10), 2151 (2010).
- [51] K. Nejati et al., *Journal of Experimental Nanoscience* 7(4), 412 (2012); <https://doi.org/10.1080/17458080.2010.538087>
- [52] J. H. Lee et al., *Chemical engineering science* 125, 75 (2015); <https://doi.org/10.1016/j.ces.2014.08.046>
- [53] D. Samaha et al., *Diss. Technol.* 16(2), 41 (2009); <https://doi.org/10.14227/DT160209P41>